Effect of ultrasound on adherent microbubble contrast agents.

Jonathan Loughran[1], Charles Sennoga[1], Robert J Eckersley[2], Meng-Xing Tang[1]

[1]Department of Bioengineering, Imperial College London, London SW7 2AZ, UK

[2]Division of Imaging Sciences, King's College London, London, SE1 7EH, UK.

Email: mengxing.tang@imperial.ac.uk

Short title: Adherent Microbubbles under Ultrasound

PACS:

87.63.D- Ultrasonography

47.55.dd Bubble dynamics

43.80.Qf Medical diagnosis with acoustics (in PACS, see also 87.63.D−)

43.80.Cs Acoustical characteristics of biological media: molecular species, cellular level tissues

Abstract

An investigation into the effect of clinical ultrasound exposure on adherent microbubbles is described. A flow phantom was constructed in which targeted microbubbles were attached using biotin-streptavidin linkages. Microbubbles were insonated by broadband imaging pulses (centred at 2.25MHz) over a range of pressures (Peak negative pressure (PNP)= 60kPa ~ 375kPa). Individual adherent bubbles were observed optically and classified as either being isolated or with a single neighbouring bubble. It is found that bubble detachment and deflation are two significant effects, even during low amplitude ultrasound exposure. Specifically, while at very low acoustic pressure (PNP < 75kPa) 95% were not affected, at medium pressure (151kPa < P < 225kPa) 53% of bubbles detached and at higher pressures (301kPa < P < 375kPa) 96% of the bubbles detached. In addition, more than 50% of bubbles underwent deflation at pressures between 301kPa and 375kPa. At pressures between 226kPa and 300kPa more adherent bubbles detached when there was a neighbouring bubble, suggesting the role of multiple scattering and secondary Bjerknes force on bubble detachment. The flow shear, primary, and secondary Bjerknes forces exerted on each bubble were calculated and compared to the estimated forces acting on the bubble due to oscillations. The oscillation force is shown to be much higher than other forces. The mechanisms of bubble detachment are discussed.

1. Introduction

While a typical ultrasound contrast agent consists of a gas bubble protected from diffusion by an encapsulating shell, targeted contrast agents add extra functionality through incorporation of binding ligands. This allows the agent to specifically bind to receptors in the body, giving them applications in both molecular imaging (Dayton and Ferrara, 2002, Lindner, 2004) and targeted drug delivery through sonoporation, when the contrast agent is combined with a drug (Unger et al., 2003). Examples of studies performed using targeted microbubbles include binding to P-Selectin, VCAM-1, VEGFR to detect inflammation for conditions such as atherosclerosis (Kaufmann et al., 2009, Lindner et al., 2001, Myrset et al., 2011) and binding to H-2Kk for tracking endothelial progenitor cells during progenitor cell treatment (Kuliszewski et al., 2009).

At present, the majority of preclinical studies of targeted microbubbles can be placed in two broad categories. The first of these is concerned with how to increase the binding efficacy of targeted microbubbles by helping them get to their binding site. These studies include using acoustic radiation force to 'push' the targeting bubbles to potential binding sites (Zhao et al., 2004a, Rychak et al., 2005, Yamakoshi and Miwa, 2009). Elsewhere, engineering strategies aimed at increasing the probability of microbubble binding has led to deflating them in order to increase their surface area and binding functionality (Rychak et al., 2006); having multiple ligands on the surface to increase their functionality (Myrset et al., 2011); increasing the density of ligands on the bubble surface; and, having buried ligands on the shell to decrease non-specific binding (Chen and Borden, 2010). The second area is concerned with using targeted microbubbles as contrast agents and trying to detect their differences and distinguish them from 'free flowing' microbubbles. These studies include using simulations (Doinikov et al., 2009, Doinikov et al., 2011, Martynov et al., 2011) and single bubble acoustic experiments (Overvelde et al., 2011, Sprague et al., 2010, Butler et al., 2008, Zhao et al., 2006) in order to investigate the acoustic properties of targeted microbubbles, image processing techniques based on temporal low pass filtering of ultrasound echo data to distinguish stationary, adherent bubbles(Needles et al., 2009, Zhao et al., 2004b) and nonlinear Doppler techniques (Mahue et al., 2011)).

A third area, which has received less attention, relates to the effect that ultrasound has on the targeted microbubbles once they bound. In a typical ultrasound acquisition the adherent bubbles within the imaging plane will be exposed to repeated ultrasound excitation at low Mechanical Index (MI, typically less than 0.2; corresponding to a pressure of 300kPa at 2.25MHz used in this study). It is not clear whether such repeated low MI pulses cause changes to the adherent bubbles and what the implications of any changes for imaging might be. As previously stated, a microbubble is bound onto its binding site through a ligand tether and a molecular binding agent. If the force exerted on the adherent microbubble is large enough then the tether may break or the molecular linkage fail, resulting in the detachment of the microbubble (Sboros et al., 2010). Studies to characterise the maximum shear under which targeted microbubbles find their binding site and also the levels of shear that remove them once they are in contact, have been conducted (Takalkar et al., 2004, Klibanov et al., 2006) and with various different bubble configurations (Ferrante et al., 2009). However, it is only recently that the detachment of targeted microbubbles due to ultrasound has been reported (Schmidt et al., 2008). The authors of this study reported that so called 'secondary Bjerknes forces' causing an attractive force between two neighbour bubbles oscillating in phase is enough to detach them. The effect of these forces was pronounced in that study as the monodisperse population used meant that each bubble oscillated in phase and so attracted all the surrounding bubbles. This effect has been further studied using high speed camera data to parameterise a model of the attraction of adherent microbubbles in comparison to unbound microbubbles in an ultrasound field (Garbin et al., 2011). This work demonstrated the effect of ultrasound on attached microbubbles in a specific situation where once again attached microbubble pairs of similar size were selected and, in this case, pulses much longer than typical imaging pulses were used.

There are other possible changes to adherent microbubbles under ultrasound. Previous studies have shown size reduction (deflation) of non-targeted microbubbles even at low acoustic pressure(Guidi et al., 2010). A change in bubble size greatly affects its efficiency as an ultrasound scatter, as a small non-resonant bubble will not give a detectable acoustic signal. Therefore, it is particularly important to study the deflation of targeted microbubbles under ultrasound, given the typically low yields of adherent bubbles in practice.

The motivation of this study is to investigate the effects of short ultrasound imaging pulses on adherent microbubbles in a flow model using optical microscopy and quantify such effects in conditions close to those used clinically. The detachment of adherent microbubbles and the forces acting on them are investigated together with the conditions that lead to deflation of the adherent microbubbles.

2. Methods

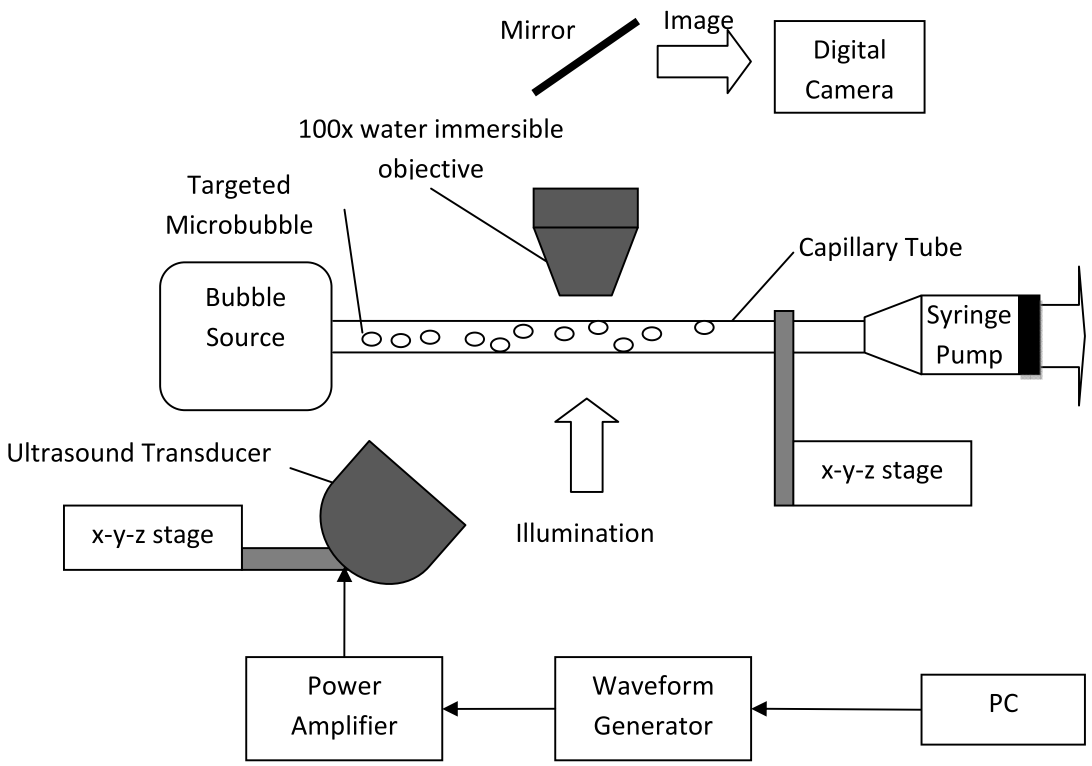

Figure 1: Schematic of the Experimental Setup

2.1 Experimental Setup

The equipment, as shown in figure 1, consisted of a 2.25MHz focused ultrasound transducer with a focal length of 75mm (Panametrics V304 , Olympus) focused onto a central point upon which a 100x water immersible objective (LUMPlanFL 100x, Olympus) was also focused. Alignment of the focuses was performed by placing a small metal sphere (a ball of solder on the end of a wire) in the focus of objective and then focusing the ultrasound transducer onto the same metal sphere aided by a 3D translation stage(Newport M-562, CA, USA). During this process the transducer was driven by a pulser/receiver operated in transmit/receive mode (Panametrics-NDT 5800) with the result displayed on a digital oscilloscope (Sony Tektronix TDS7154). This alignment of the optics and acoustics ensures that the microbubbles in view during the experiment are being insonated at the pressures measured at the ultrasound focus. The size of the optically viewable area is approximately 0.1mm by 0.1mm while the ultrasound focus is about 1mm by 1mm, and thus the acoustic focus is substantially larger than the optical field of view. A 200μm inner diameter cellulose tube (RC55 8/200 Membrana GmbH) coated with streptavidin was then placed into the focus using another identical 3D translation stage.

A burst of 30 Gaussian enveloped broadband sinusoidal pulses (full width half maximum of 1μs) was generated by a programmable waveform generator (Sony Tektronix AWG2021) taking an input from an in-house triggering software written in Matlab (Mathworks, Cambridge UK). The burst was amplified by a power amplifier (E&I 2100L) to drive the transducer over a one second period (pulse repetition frequency 30 Hz) followed by a 0.5 second pause before increasing the output pressure and repeating, five times in total to form a six-step pressure ramp. A calibrated needle hydrophone (HPM1/1 Precision Acoustics, Dorset, UK) was used to calculate the pressures at the focal point of the ultrasound transducer. A total of two separate pressure ramps were employed with the maximum insonation pressure of 370kPa (peak negative pressure, accurate to ±13%, corresponding MI=0.25) and 300kPa (MI = 0.20) respectively.

Light from the microscope objective was collected via a digital camera (Powershot A95, Canon) with a frame size of 640x480 pixels at 10 frames per second, after the light from the objective being reflected through a mirror at 45 degrees and a focusing lens. The magnification of the image obtained was controlled by changing the distance between the focusing lens and the camera lens and also by adjusting the distance between the mirror and the camera to obtain an optical view of approximately 100μm x 76μm with a resolution of 0.32μm per pixel. Optical sizing was calibrated by manually measuring the diameter of in-focus 5μm latex calibration beads (L5 microspheres, Meritics Ltd). In order to calculate tolerances of the sizing process, the beads were repeatedly sized at varying degrees of focus. The standard error was found to be 16% of the bubble diameter and the location of the bubble centre was found to be accurate to within one pixel. To be able to distinguish when the microbubbles were exposed to the acoustic field, the clocks on the PC triggering the ultrasound generation and digital camera were synchronised. Before triggering the ultrasound transmission, the video mode of the digital camera was manually triggered. Video data was then captured for the duration of the ultrasound sequence until no further change in the status of the targeted microbubbles could be visually observed.

In order to verify that the microbubbles were adherent to the walls of the tube, experiments were performed under flow conditions using a syringe pump in withdraw mode. In this situation any unattached bubbles were observed to flow away. To both maximise the number of bubbles binding to the tube, and to enable the free flowing unbound bubbles in the tube to be seen, a relatively low flow rate of 3μl/min was used. A flow rate was selected, empirically, that was high enough to stop bubbles from coming to a stop by themselves, but low enough that the shear rate caused by the flow did not lead to observable detachment of adherent bubbles. Shear rates resulting from the flow and their effects are discussed later.

2.2 Microbubble and Tube Preparation

Microbubbles were prepared by sonication (Misonix Sonicator 3000, 21kHz 165W; 30sec) of an aqueous suspension of distearoyl-phosphatidylcholine, distearoyl-phosphatidylethanolamine-PEG2000-biotin and poly(ethyleglycol)-monostearate saturated with octafluoropropane gas. Lipids not incorporated into the microbubble shells were removed by repeated (5 times) centrifugal washing (4°C; 160 rcf; 4 minutes) of the targeted microbubble dispersion in gas-stabilised ISOTON II saline (Coulter Electronic Ltd, Bedfordshire, UK) using a desk-top Rotanta 460R bucket-type rotor (Andreas Hettich GmbH, Tuttlingen, Germany). The size distribution and concentration of targeted microbubbles was reproducibly determined and returned a mean diameter of 2.4 (±0.4)μm and a concentration of 1.2×10^9 microbubbles/ml using optical microscopy (Sennoga et al., 2010).

To coat the cellulose tubes one end was placed in a streptavidin (Invitrogen Life Technologies Ltd, UK) solution at a concentration of 0.25 mg/ml. The solution was taken up by the tube through capillary action. The tubes that were intended for use on that day were incubated at room temperature for at least 2 hours, and those for use at a later date were stored in a hydrated sealed container at 5 °C to stop them from drying out. Before being used in an experiment the remaining streptavidin solution was wicked out of the tube using a piece of tissue paper and the two ends of the tube were inserted and glued into two 25 gauge butterfly needles (246.052, Vygon) thus allowing the tube to be connected to a bubble reservoir on one end and a syringe pump (SP210iwZA, World Precision Instruments) on the other. Finally, the remaining unbound streptavidin solution was removed from the tube by pumping 2ml of sterilised PBS (Sigma-Aldrich Ltd. Dorset, UK) through the tube. This process is required as any remaining streptavidin free flowing through the tube at the time of the experiment could potentially block the ligands on the targeted microbubbles before they have a chance to find their target.

2.3 Data Analysis

An in-house MATLAB program was designed to extract the information from the videos collected. The objective of the software was to size the bubbles and also track their coordinates for the duration of the ultrasound exposure. The process for data processing for each video was as follows:

1. Each adherent bubble was visually identified and three points on the circumference were manually selected. From this the initial size and central coordinates of each bubble were calculated.
2. On each of the following frames cross correlation was used after thresholding to automatically track the movement of each bubble between frames. In the event of the bubbles new position successfully being located, the bubbles were automatically sized using automated optical sizing software(Sennoga et al., 2010). In the result of the tracking algorithm failing to identify a new location, the bubbles were manually sized again as described in step 1. At the end of each frame the diameters of each bubble were then reviewed and any automatic sizing errors (such as false positives in tracking), were corrected by user intervention.
3. To reduce the effects of sizing errors in the calculations for forces (due to the bubble moving out of focus or moving), a 5 element moving averaging filter was applied to the time sampled sizing data.
4. The data from individual bubbles was then further categorized into two classes; either “detachment” when a previously static bubble was observed to move between frames, or “survival” when a bubble was unchanged at the end of a ultrasound burst. For each event the time of the event, the ultrasound pressure, bubble size, size of its nearest neighbour and distance from its nearest neighbour were recorded. For any bubble that detached at lower pressure it was assumed that the same bubble would have been detached by higher pressures. A sample of data extracted from a single video is shown in figure 2.

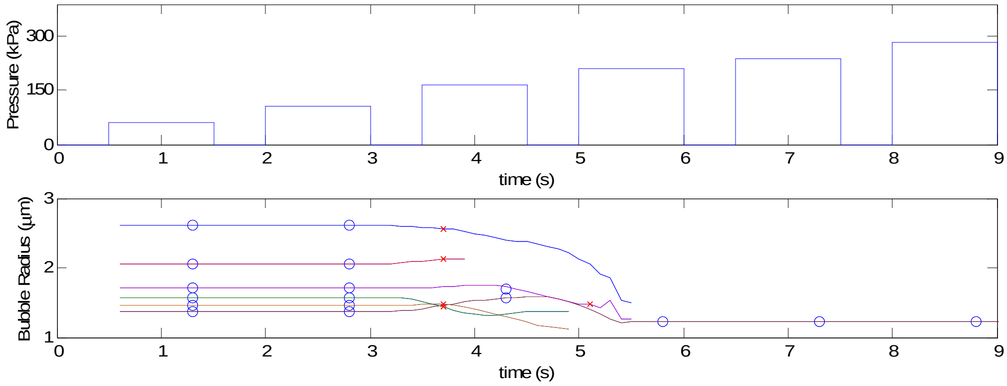

Figure 2: a) Illustration of the pulse sequence. b) Diameters of bubbles against time. An ‘x’ indicates a detachment event, and a ‘o’ indicates a survival event. Bubbles were sized to ±16% of real bubble size. Locations of bubbles are accurate to ±0.32μm (These values were determined through tests of the sizing carried out on 5μm calibration beads).

5. Finally, a reduction in bubble diameter between observations of more than 20% was recorded as deflation of the bubble. As above with the case of bubble detachments, a bubble deflated at a lower pressure was assumed to deflate at higher pressures.

2.4 Force Calculations

The detachment of adherent microbubbles is related to the various forces acting on the microbubbles, as well as a number of other factors such as the nature, number, length and relative positions of the ligands involved and whether they are under tension or not (Chen and Borden, 2010, Ferrante et al., 2009). In this study we concentrate on the calculation of the various forces acting on the microbubbles, other factors are discussed in the discussion section.

2.4.1 Use of Experimental Data in Force Simulations

Data gathered from the video processing, the bubble size and locations are directly used to calculate the forces on each bubble. The selection of bubble parameters used for the simulation is as follows. In the case of a detachment event, the bubble size and location are used in the video frame before visible detachment can be identified. In the case of a survival event, the bubble size and location at the end of the burst survived are used. The bubble radii at these time points are then used to calculate bubble oscillations and the incident forces described below.

When viewed in terms of a translational force, the Bjerknes force is usually considered as an average of forces over a complete cycle (hence the time averaging). However, when considering the rupture of binding ligands, the processes is a much shorter term event, meaning that the maximum, instantaneous, force exerted is more relevant to our study than the mean force over a single cycle.

2.4.2 Shear Forces

The force of the fluid pushing its way past the adherent bubbles may be enough to remove them from their binding site given a large enough flow gradient at the edges of the flow. The general formula for shear stress τ for a Newtonian fluid in a pipe is $\tau = \mu \, {}^{\delta v}/_{\delta x}$, where μ is the fluid viscosity and v is the flow velocity(Batchelor, 2000). The shear forces were calculated by tracking the speed of in focus free bubbles across the videos.

2.4.3 Primary Bjerknes Force

The primary Bjerknes force also known as the acoustic radiation force, describes the translation of an object in an acoustic field due to local pressure changes (Crum and Eller, 1970, Leighton, 1990). Although the application of this theory in our paper is with regard to bubbles, primary Bjerknes forces act on any inhomogenities in an acoustic field.

Given a body with a volume V in a pressure gradient ∇P the net force applied is the time average of this, namely:

$$F_{PB} = -\langle V(t)\nabla P(r,t)\rangle \quad (1)$$

Where $\langle \quad \rangle$ denotes an average over time. In the case of the encapsulated microbubbles the volume is time dependant as the bubble oscillates in the acoustic field. Ignoring effects such as shell buckling, shell shear thinning etc. this change in volume can be described in terms of the bubble radius R, using an extended version of the Rayleigh-Plesset equation to include the basic properties of the bubble shell (Doinikov and Bouakaz, 2011):

$$\rho\left(R\ddot{R} + \frac{3}{2}\dot{R}^2\right) = \left(P_0 + \frac{2\sigma}{R_0} - P_v\right)\left(\frac{R_0}{R}\right)^{3\kappa} - \frac{2\sigma}{R} - \frac{4\mu}{R} - \frac{4\kappa_s\dot{R}}{R^2} - \frac{4\chi(R-R_0)}{R^2} - P_0 - P(t) \quad (2)$$

Where ρ is the density of the surrounding fluid, σ is the surface tension, μ is the dynamic viscosity of the surrounding fluid, κ is the polytropic constant, κ_s is the shell's dilatational viscosity, χ is the shell's elastic modulus, P_0 is the hydrostatic pressure, P_v is the vapour pressure inside the bubble and R_0 is the initial bubble size. Based on the fact that the primary Bjerknes force is being applied to a bubble equation 1 can be rewritten as:

$$F_{PB} = -\frac{4\pi}{3}R(t)^3 \, \frac{\partial P(r,t)}{\partial r} \quad (3)$$

In previous studies (Dayton et al., 1997, Doinikov and Dayton, 2006) the primary Bjerknes force was calculated by treating the bubble as a linear oscillator with a known resonant frequency and amplitude of oscillation and a time average was performed analytically over one cycle of a continuous wave oscillation. This study has taken a different approach; firstly the microbubbles in the simulation are driven by a pulse derived from measured data. This reduces error in the calculation of the simulated force. This change also allows for the calculation of instantaneous force as opposed to an averaged force over whole cycle. This fact is used later in calculating the maximum force undergone by the bubble. When considering the translation of a bubble, the average force over a cycle is important to show the overall translation of the bubble, however, when dealing with the breaking of bonds such as in our case, it is the impulse that are the most likely to have an effect. Secondly, due to the proximity of the boundary wall, the bubble cannot be simply viewed as a linear oscillator with a known resonant frequency. Therefore, in calculating the extent of the primary Bjerknes forces, the radius-time curve is calculated for each bubble and put into equation (3) where the resulting force is given as the mean of F_{PB} observed over a single oscillation. In order to take into account the effect of the boundary on the oscillations of the bubble, a further term was added to equation (2) using image bubble theory (Doinikov et al., 2009).

$$\rho\left(R\ddot{R}+\frac{3}{2}\dot{R}^2\right)=\left(P_0+\frac{2\sigma}{R_0}-P_v\right)\left(\frac{R_0}{R}\right)^{3\kappa}-\frac{2\sigma}{R}-\frac{4\mu}{R}-\frac{4\kappa_s\dot{R}}{R^2}-\frac{4\chi(R-R_0)}{R^2}-P_0-P(t)-\left(R\ddot{R}+2\dot{R}^2\right)\frac{R\rho\beta}{2x} \tag{4}$$

Where *x* is the distance of the bubble centre from the boundary, and *β* is the percentage of the pressure reflected off the boundary that interferes with the bubble. *β* was set to 0.2 based on a similarly motivated simulation carried out on a similar experimental setup (Garbin et al., 2011) and *x* was set to R_0. As for the properties of the bubbles themselves, κ_s was $5x10^{-9}$N and χ, 0.1Nm^{-1}. These values were obtained by matching the simulated results to experimental measurements of attached targeted microbubbles obtained through single bubble acoustic experiments under the same conditions (Casey et al., 2012).

2.4.4 Secondary Bjerknes Forces

The secondary Bjerknes force occurs due to the pressure changes between two oscillating objects (Crum, 1975, Leighton, 1994). When they oscillate in phase a negative pressure gradient between the objects is formed attracting them together, however when they oscillate out of phase a positive pressure gradient is formed repelling the two oscillators away from each other. A formula for the secondary Bjerknes forces is given by:

$$F_{SB}=-\frac{4}{3}\pi\rho R_1^3\frac{\ddot{R}_2R_2^2+\dot{R}_2^2R_2}{d^2} \tag{5}$$

Where $R_1$is the radius of the bubble the force is being acted upon, R_2 is the radius of R_1's neighbouring bubble and d is the separation between the two bubbles. Again as with the primary Bjerknes forces the Rayleigh-Plesset equation (equation (4)) was used to calculate the oscillations of the microbubbles given the derived shell properties as detailed in the previous section and the measured acoustic pulse. Equation 5 can be used to calculate the instantaneous force that the bubble undergoes and not just a time averaged force over a single cycle. Although in the data gathered there were multiple bubbles at any one point in time, only a single nearest neighbour was used to calculate the secondary Bjerknes force. Even though groups of bubbles do show secondary Bjerknes forces between them, the calculation of the complex interactions that create the pressure fields between several neighbouring bubbles is beyond the scope of this study. It is worth noting that the secondary Bjerknes force between two bubbles is inversely proportional to the square of the distance between them, resulting in a significant reduction in the influence of neighbouring bubbles at greater distance.

2.4.5 Bubble Oscillation Forces

The bubble oscillates due to the imbalance of various forces acting on it. The right hand side (RHS) of equation 4 describes the summation of the various pressures acting on a bubble which results in the motion of the bubble and its surrounding fluid (the left hand side (LHS) of equation 4). Such oscillation moves the bubble shell and the associated force may be able to stretch and break the bonds between the bubble and the wall. In this document we have named this force the bubble oscillation force as it comes into play through the inertia of the surrounding fluid when the bubble is under oscillation. The magnitude of this force acting on the wall of the bubble as it expands and contracts is the product of the pressure due to the fluid inertia (LHS of equation 4) and the bubble cross-section and is described by equation 6,

$$F_{Osc} = \pi R^2 \left(R\ddot{R} + \frac{3}{2}\dot{R}^2 \right) \rho \qquad (6)$$

This equation was derived by integrating the inertia forces over the bubble in a similar fashion to calculating the surface tension by summing the local forces making it up (Leighton, 1994). Although this oscillation force is not the same as the actual force acting on the ligand when the bubble oscillates, calculating such force can still offer an indication of the scale of the force involved.

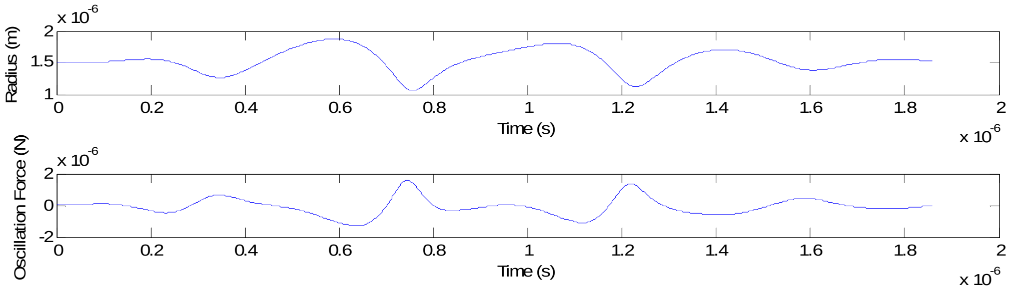

Figure 3: Oscillations and associated oscillation forces experienced by a 3μm bubble. Positive forces correspond to an expansion, while negative forces correspond to a compression.

3. Results

3. 1 Description of the overall data set

The experiment detailed in the methods section was carried out a total of 42 times and a total of 229 bubbles were identified and tracked. From these experiments 1894 detachment events were generated using the process described in section 2.3.

3.2 Detachment in Single Bubble Environments

From 1894 separate events taken from the data set, 367 cases were highlighted where a bubble was isolated in the experiment. This includes situations where there was only one bubble in the experiment from the start, or all other bubbles at the start of the relevant ultrasound burst have been destroyed or have detached and vanished from view, or cases where there is no bubble within a 20 radii zone around the bubble (the distance at which bubble-bubble interactions are considered to be negligible (Garbin et al., 2009)). The motivation for analysing this subset of the data is to examine the detachment of bubbles without influence of the secondary Bjerknes forces.

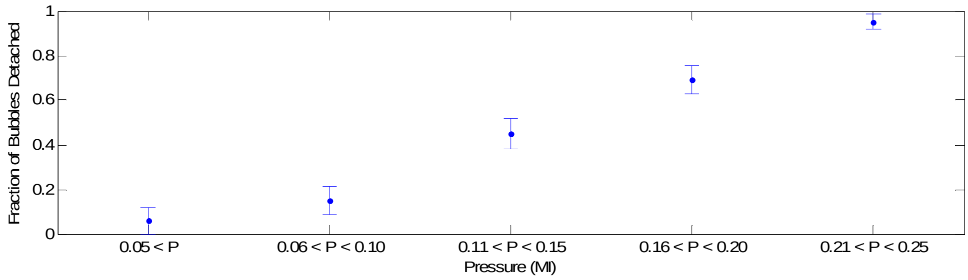

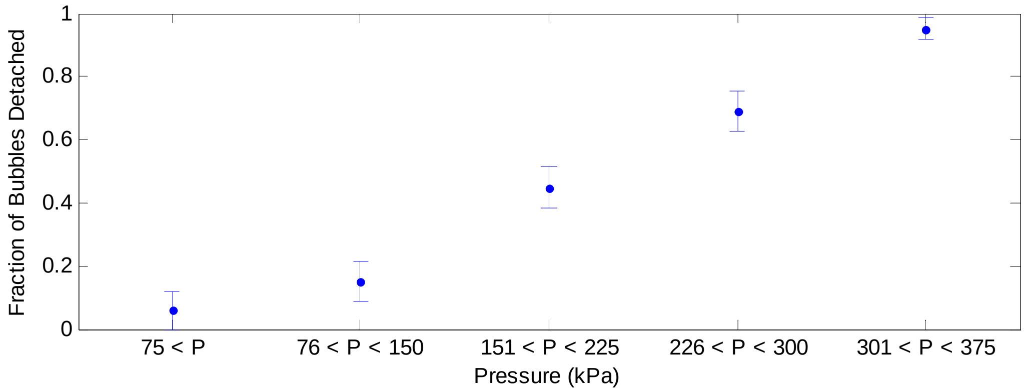

Figure 4: Rate of bubble detachment for increasing acoustic pressures on single adherent bubbles error given is standard error across each video.

Figure 4 demonstrates the effect of increasing acoustic pressure on the detachment of targeted bubbles. The y-axis of this graph is calculated using equation (7):

$$\text{Fraction of Bubbles Detached} = \frac{\text{No.of detachment events}}{\text{Total no.of events}} \qquad (7)$$

It can be seen that even with MIs between 0.11 and 0.15 more than half of the adherent microbubbles detach. This fraction of detachment increases to 96% at pressuress between 301kPa and 375kPa.

3.3 Detachment in Multiple Bubble Environments

1518 multiple bubble events were recorded and analysed. In these cases, bubbles are affected by secondary Bjerknes forces in addition to those forces acting on isolated bubbles.

Comparing the single and multiple bubble environments, a 2 way t-test shows a significant difference between the detachment for single and multiple bubbles in the pressure range of 226kPa < P < 300kPa.

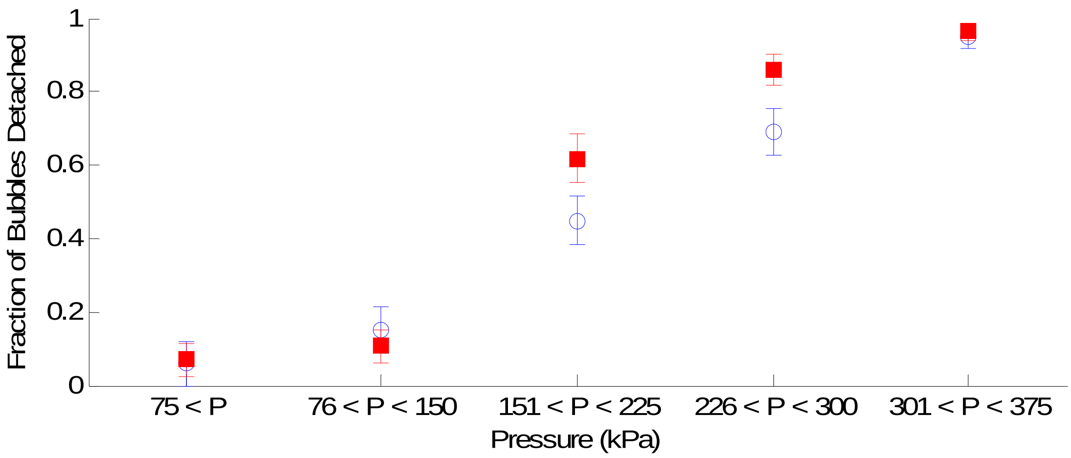

Figure 5: Detachment rates for increasing pressures. O: Single bubble environments, ■: Multiple bubble environments.

3.4 Deflation of Targeted Microbubbles

Out of the 794 survival events identified, 202 were found to be in single bubble environments, and the remaining 592, were in multiple bubble environments. The rate of deflation for the attached bubbles is shown in figure 6.

$$\text{Fraction of Attached Bubbles Deflated} = \frac{\text{No.of deflation events}}{\text{Total no.of events}} \qquad (8)$$

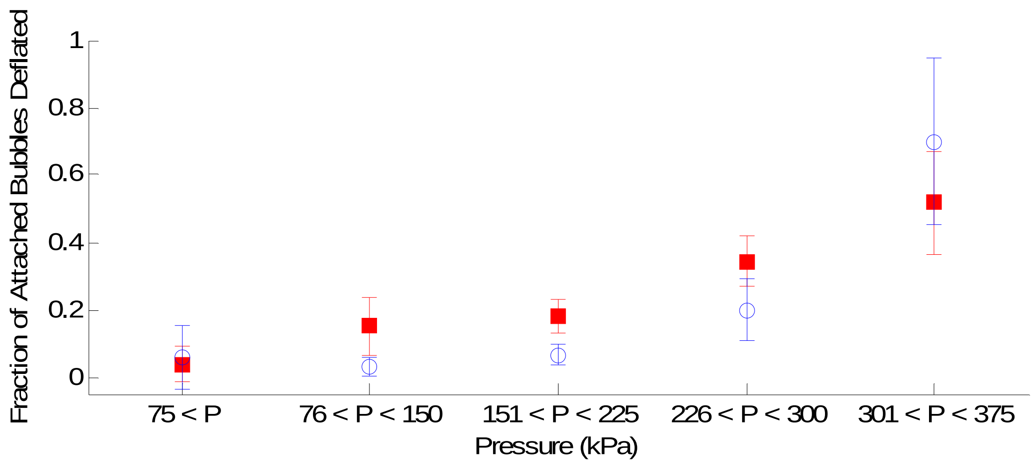

Figure 6: Deflation rates for attached bubbles at increasing pressures. O: Single bubble environments, ■: Multiple bubble environments.

Note that deflation is treated to be completely independent from detachment as an event, and so while all bubbles started off attached, some bubbles stayed in place and some became detached during the deflation process as stated in 3.1. Statistically, no significant difference was found to exist between the single bubble and multiple bubble environments.

4. Discussion

In this study the effects of low amplitude ultrasound on adherent microbubbles were found to be significant. Both detachment and deflation of adherent microbubbles were observed. Specifically the detachment of bubbles was found to be the most significant effect, affecting the majority of adherent bubble population at pressuress from as low as 151kPa. To obtain some further insight into the mechanisms of bubble detachment, the magnitude of the various forces acting on each of the observed bubble was calculated and their effects discussed.

4.1 Effects of the forces in bubble detachment

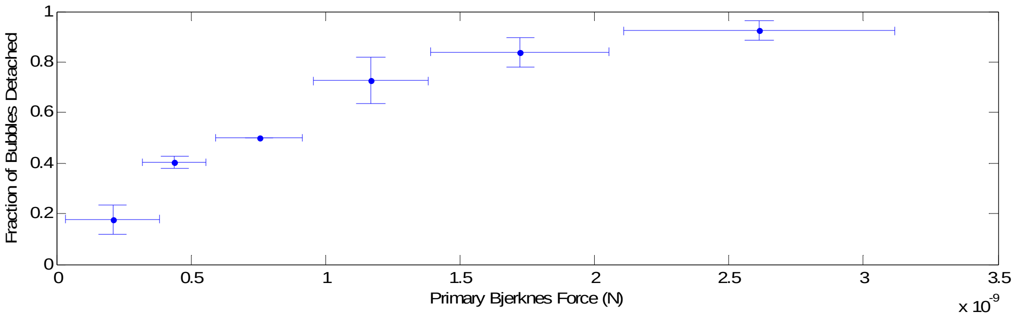

Figure 7: Number of adherent bubbles detached verses primary Bjerknes force on single adherent bubbles.

Figure 7 displays the link between the primary Bjerknes force and detachment rates for the set of single bubbles. In the experiment the tube was placed perpendicular to the direction of the acoustic field, meaning that the direction of the primary Bjerknes force experienced by each bubble was across the tube, i.e. perpendicular to the wall the bubbles were bound to. Any change in the ultrasound field's orientation would lead to a change the direction of primary Bjerknes forces and have an effect on the detachment levels. While on this note, it is worth discussing the relationship between the two forces. The shear force acting on a bubble is directly dependant on the cross sectional area, and so the larger the bubble the larger the force acting on it. Whereas the primary Bjerknes force depends on whether the bubble is being driven at resonance and the pressure it is exposed to. The larger the volume of the oscillations the larger the force that the bubble experiences.

Figure 8 presents the results overlaid on a simulation showing the primary Bjerknes forces over a range of bubble sizes and pressures. The figure shows that the resonant bubbles are the first to be detached whilst those far away from resonance remain resilient. This has particular implications for the clinical use of targeted microbubbles, as under some clinical investigative pressures (around 0.2MI) 89% of the targeted bubbles at resonance (ie. also corresponding to those visible under ultrasound) will become detached under the same orientations as those used in our experiment. It is worth noting at this point that when targeted microbubbles have been attached using acoustic radiation force, the primary radiation force is pushing the bubbles into the wall and so this associated detachment will not be present. However, in this situation other forces including secondary Bjerknes forces will still contribute to the detachment of targeted microbubbles.

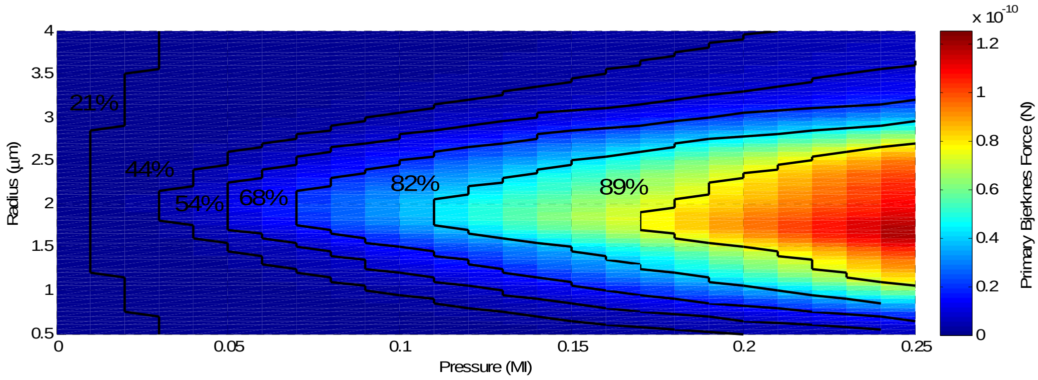

Figure 8: Simulated primary Bjerknes force (colour bar) vs. acoustic pressure and bubble radius. Black lines display the experimentally observed detachment rates.

At this point it is worth comparing the primary Bjerknes force as an averaged and an instantaneous force. For a 4.2μm bubble, while the average primary Bjerknes force experienced in a single cycle is 5.3pN, the maximum force undergone is 1.3nN, several orders of magnitude higher.

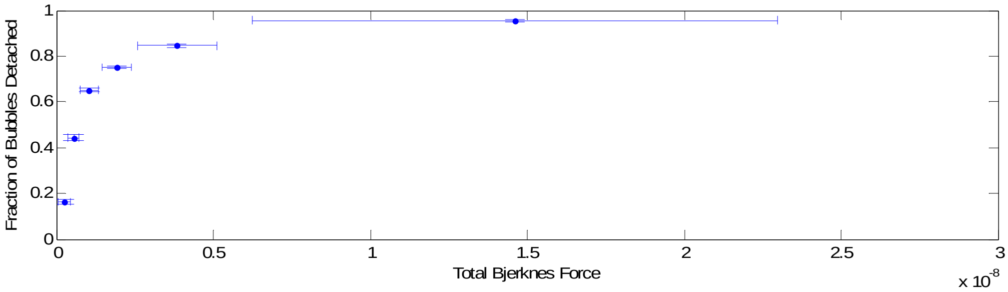

Figure 9: Detachment rates against the sum of both primary and secondary Bjerknes forces.

While secondary Bjerknes forces have an influence on bubble detachment, it is not possible to isolate the individual forces acting on the bubbles, especially in the situation where bubble-bubble interactions are occurring. Therefore the detachment of bubbles must be considered in terms of the sum of both the primary and secondary Bjerknes forces when considering the acoustic forces. Figure 9 shows an increasing rate of detachment with increasing total Bjerknes force. Another mechanism that may contribute to the detachment of microbubbles is the violent bubble oscillations breaking the ligand bonds. This kind of effect would be dependent on the resonant behaviour of the microbubble itself, similar to that of the primary Bjerknes forces making the two effects indiscernible. Also in situations where there are multiple bubbles together increased oscillations from multiple scattering could also explain increased detachment rates.

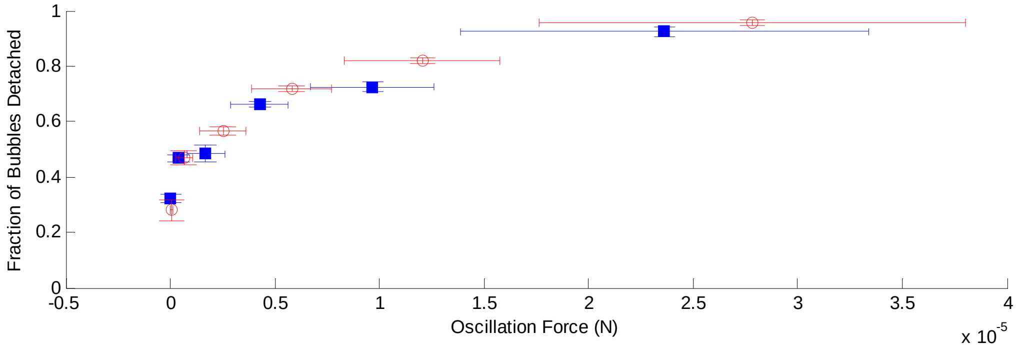

Figure 10: Oscillation force against detachment rates. O: Single bubble environments, ■: Multiple bubble environments.

The results show that the magnitude of the oscillation force in this experiment was much higher than that of the Bjerknes forces.

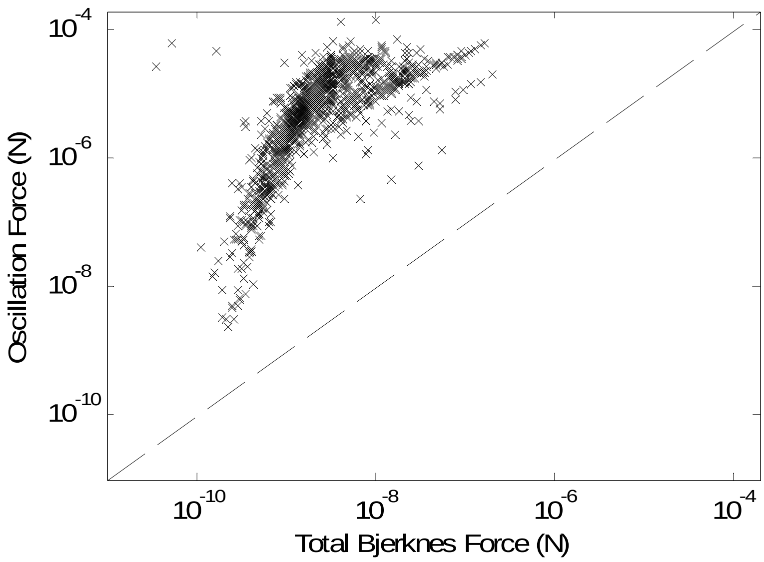

Figure 11: Relationship between Oscillation forces and Bjerknes forces for individual detached bubbles. The dotted line denotes equal magnitude in both forces.

Three forces involved in the detachment of microbubbles have been studied; namely, primary and secondary Bjerknes and oscillation forces, while the effect of shear forces was minimised in this study. The oscillation force is calculated to be much larger than the Bjerknes forces, but the effect of this oscillation force is shorter in time scale than the other forces as it does not have a net effect over cycles. The contribution of each force to bubble detachment is related to both the force magnitude and the time scale. If some ligands are folded in the beginning (under zero tension), it might take the shear/Bjerknes forces to unfold the ligands and put them under tension before the oscillation force can break the bonds.

4.2 Implications of Bubble Deflation and Detachment

Attached microbubbles were observed to deflate with increasing rates as acoustic pressure was increased, with more than 50% of bubbles experiencing deflation to some degree for pressures greater than 300kPa. This has major implications for molecular imaging as, if this reaction was observed acoustically via an ultrasound scanner it could give the appearance than the bubble has been destroyed as it scattering profile is reduced to the point that it is no longer visible. These bubbles could then remain in place and invisibly occupy binding sites. This would introduce a bias in the quantification of molecular imaging, were the number of microbubbles bound to a site is compared across studies. The same implications can be said to be true when considering bubble detachment; when a bubble detaches the remaining parts of the bubble may stay in place stopping another bubble taking position at the site. On top of this, any movement of a bubble away from the site reduces its effectiveness as a molecular imaging agent.

4.3 Limitations

In this study the orientation of the ultrasound field generates primary Bjerknes force that shears the bubble against the vessel wall. Changing the orientation of the ultrasound field would change the direction of the primary Bjerknes forces. If for example the primary Bjerknes forces were pushing the bubble in the same direction as the wall they are bound to, the effect of the primary Bjerknes force on detachment will be considerably lower than that reported in this paper.

Another limitation in this study is that the equations used to calculate the oscillation force do not take into account the kind of translational and/or asymmetrical oscillation that a bubble undergoes when in the vicinity of a vessel wall(Vos et al., 2008). Therefore further studies such as FEM modelling of targeted microbubbles adherent to a wall would be required in order to obtain further insight into the detachment process.

Although some targeted microbubble were exposed to ultrasound on multiple separate occasions, the time between pulses (one thirtieth of a second) and the gap between bursts (half a second) is long comparing to the oscillations and gas diffusion process. However, as far as the strength of the bond is concerned one could argue that an attached microbubble has been ‘massaged’ by the previous lower power bursts causing a detachment, where originally the bubble would have stayed attached. While this is a limitation in the experimental design, the experiment was carried out in this way to improve the efficiency of data collection, as it was deemed impractical to expose each microbubble to only a single burst. However, it should also be noted that the inclusion of multiple event data from the same individual bubbles has unknown implications on the statistical independence of the data and further independent measurements maybe needed to confirm the statistical findings.

5. Conclusion

This study investigated the effect of an ultrasound field on adherent microbubbles. It was shown that at very low acoustic pressure (< 75kPa) most adherent bubbles remained unaltered under flow. However, a significant amount of adherent bubbles were detached and/or deflated as the pressure was increased. At pressures> 300kPa 96% of the bubbles detached. Three separate forces acting on the bubbles were investigated regarding their role in the process of bubble detachment. The force from bubble oscillations was found to be the largest force acting on the attached bubbles. At acoustic pressures (pressure=226kPa~300kPa) more adherent bubbles detached when there was a close neighbouring bubble, suggesting a role of multiple scattering and secondary Bjerknes Force in bubble detachment. Finally, 56% of attached microbubbles were found to deflate when insonated at pressures > 300kPa, although, no difference was found in the deflation of single and multiple bubble environments. The recommendations of this study are that targeted microbubbles should be imaged with a low pressure as possible in order to minimise the adverse effects of ultrasound.

Acknowledgements

The authors would like to thank, Eleanor Stride, David Cosgrove, Helen Mulvana, Jonathan Casey and Richard Browning for their valuable advice in helping to design the experiment. This work was funded by EPSRC grant number EP/G038163/1.

References

BATCHELOR, G. K. 2000. *An Introduction to Fluid Dynamics*, Cambridge University Press.

BUTLER, M. B., THOMAS, D. H., PYE, S. D., MORAN, C. M., MCDICKEN, W. N. & SBOROS, V. 2008. The acoustic response from individual attached and unattached rigid shelled microbubbles. *Applied Physics Letters,* 93.

CASEY, J., SENNOGA, C. A., MULVANA, H., HAJNAL, J. V., TANG, M.-X. & ECKERLSEY, R. J. 2012. Single Bubble Acoustic Characterisation and Stability Measurement of Adherent Microbubbles. *Ultrasound in Medicine & Biology*.

CHEN, C. C. & BORDEN, M. A. 2010. Ligand Conjugation to Bimodal Poly(ethylene glycol) Brush Layers on Microbubbles. *Langmuir,* 26**,** 13183-13194.

CRUM, L. A. 1975. Bjerknes Forces on Bubbles in a Stationary Sound Field. *Journal of the Acoustical Society of America,* 57**,** 1363-1370.

CRUM, L. A. & ELLER, A. I. 1970. Motion of Bubbles in a Stationary Sound Field. *Journal of the Acoustical Society of America,* 48**,** 181-&.

DAYTON, P. A. & FERRARA, K. W. 2002. Targeted imaging using ultrasound. *Journal of Magnetic Resonance Imaging,* 16**,** 362-377.

DAYTON, P. A., MORGAN, K. E., KLIBANOV, A. L. S., BRANDENBURGER, G., NIGHTINGALE, K. R. & FERRARA, K. W. 1997. A preliminary evaluation of the effects of primary and secondary radiation forces on acoustic contrast agents. *Ieee Transactions on Ultrasonics Ferroelectrics and Frequency Control,* 44**,** 1264-1277.

DOINIKOV, A. A., AIRED, L. & BOUAKAZ, A. 2011. Acoustic scattering from a contrast agent microbubble near an elastic wall of finite thickness. *Physics in Medicine and Biology,* 56**,** 6951-6967.

DOINIKOV, A. A. & BOUAKAZ, A. 2011. Review of shell models for contrast agent microbubbles. *Ultrasonics, Ferroelectrics and Frequency Control, IEEE Transactions on,* 58**,** 981-993.

DOINIKOV, A. A. & DAYTON, P. A. 2006. Spatio-temporal dynamics of an encapsulated gas bubble in an ultrasound field. *Journal of the Acoustical Society of America,* 120**,** 661-669.

DOINIKOV, A. A., ZHAO, S. & DAYTON, P. A. 2009. Modeling of the acoustic response from contrast agent microbubbles near a rigid wall. *Ultrasonics,* 49**,** 195-201.

FERRANTE, E. A., PICKARD, J. E., RYCHAK, J., KLIBANOV, A. & LEY, K. 2009. Dual targeting improves microbubble contrast agent adhesion to VCAM-1 and P-selectin under flow. *Journal of Controlled Release,* 140**,** 100-107.

GARBIN, V., DOLLET, B., OVERVELDE, M., COJOC, D., DI FABRIZIO, E., VAN WIJNGAARDEN, L., PROSPERETTI, A., DE JONG, N., LOHSE, D. & VERSLUIS, M. 2009. History force on coated microbubbles propelled by ultrasound. *Physics of Fluids,* 21.

GARBIN, V., OVERVELDE, M., DOLLET, B., DE JONG, N., LOHSE, D. & VERSLUIS, M. 2011. Unbinding of targeted ultrasound contrast agent microbubbles by secondary acoustic forces. *Physics in Medicine and Biology,* 56, 6161-77.

GUIDI, F., VOS, H. J., MORI, R., DE JONG, N. & TORTOLI, P. 2010. Microbubble characterization through acoustically induced deflation. *IEEE Trans Ultrason Ferroelectr Freq Control,* 57, 193-202.

KAUFMANN, B. A., CARR, C. L., BELCIK, J. T., XIE, A., YUE, Q., CHADDERDON, S., CAPLAN, E. S., KHANGURA, J., BULLENS, S., BUNTING, S. & LINDNER, J. R. 2009. Molecular Imaging of the Initial Inflammatory Response in Atherosclerosis. Implications for Early Detection of Disease. *Arterioscler Thromb Vasc Biol*, ATVBAHA.109.196386.

KLIBANOV, A. L., RYCHAK, J. J., YANG, W. C., ALIKHANI, S., LI, B., ACTON, S., LINDNER, J. R., LEY, K. & KAUL, S. 2006. Targeted ultrasound contrast agent for molecular imaging of inflammation in high-shear flow. *Contrast Media & Molecular Imaging,* 1, 259-266.

KULISZEWSKI, M. A., FUJII, H., LIAO, C., SMITH, A. H., XIE, A., LINDNER, J. R. & LEONG-POI, H. 2009. Molecular imaging of endothelial progenitor cell engraftment using contrast-enhanced ultrasound and targeted microbubbles. *Cardiovascular Research,* 83, 653-662.

LEIGHTON, T. G. 1990. Primary Bjerknes forces. *European Journal of Physics,* 11, 50.

LEIGHTON, T. G. 1994. *The Acoustic Bubble*, Academic Press Inc.

LINDNER, J. R. 2004. Molecular imaging with contrast ultrasound and targeted microbubbles. *J Nucl Cardiol,* 11, 215-21.

LINDNER, J. R., SONG, J., CHRISTIANSEN, J., KLIBANOV, A. L., XU, F. & LEY, K. 2001. Ultrasound Assessment of Inflammation and Renal Tissue Injury With Microbubbles Targeted to P-Selectin. *Circulation,* 104, 2107-2112.

MAHUE, V., MARI, J. M., ECKERSLEY, R. J. & TANG, M.-X. 2011. Comparison of Pulse Subtraction Doppler and Pulse Inversion Doppler. *Ieee Transactions on Ultrasonics Ferroelectrics and Frequency Control,* 58, 73-81.

MARTYNOV, S., KOSTSON, E., SAFFARI, N. & STRIDE, E. 2011. Forced vibrations of a bubble in a liquid-filled elastic vessel. *The Journal of the Acoustical Society of America,* 130, 2700-2708.

MYRSET, A. H., FJERDINGSTAD, H. B., BENDIKSEN, R., ARBO, B. E., BJERKE, R. M., JOHANSEN, J. H., KULSETH, M. A. & SKURTVEIT, R. 2011. Design and Characterization of Targeted Ultrasound Microbubbles for Diagnostic Use. *Ultrasound in Medicine & Biology,* 37, 136-150.

NEEDLES, A., COUTURE, O. & FOSTER, F. S. 2009. A method for differentiating targeted microbubbles in real time using subharmonic micro-ultrasound and interframe filtering. *Ultrasound in Medicine and Biology,* 35, 1564-1573.

OVERVELDE, M., GARBIN, V., DOLLET, B., DE JONG, N., LOHSE, D. & VERSLUIS, M. 2011. Dynamics of Coated Microbubbles Adherent to a Wall. *Ultrasound in Medicine & Biology,* 37, 1500-1508.

RYCHAK, J. J., KLIBANOV, A. L. & HOSSACK, J. A. 2005. Acoustic radiation force enhances targeted delivery of ultrasound contrast microbubbles: in vitro verification. *IEEE Trans Ultrason Ferroelectr Freq Control,* 52, 421-33.

RYCHAK, J. J., LINDNER, J. R., LEY, K. & KLIBANOV, A. L. 2006. Deformable gas-filled microbubbles targeted to P-selectin. *Journal of Controlled Release,* 114, 288-299.

SBOROS, V., GLYNOS, E., ROSS, J. A., MORAN, C. M., PYE, S. D., BUTLER, M., MCDICKEN, W. N., BROWN, S. B. & KOUTSOS, V. 2010. Probing microbubble targeting with atomic force microscopy. *Colloids and Surfaces B-Biointerfaces,* 80, 12-17.

SCHMIDT, B. J., SOUSA, I., VAN BEEK, A. A. & BOHMER, M. R. 2008. Adhesion and ultrasound-induced delivery from monodisperse microbubbles in a parallel plate flow cell. *Journal of Controlled Release,* 131, 19-26.

SENNOGA, C. A., MAHUE, V., LOUGHRAN, J., CASEY, J., SEDDON, J. M., TANG, M.-X. & ECKERSLEY, R. J. 2010. On Sizing and Counting of Microbubbles using Optical Micoscropy. *Ultrasound in Medicine and Biology,* 36**,** 2093-2096.

SPRAGUE, M. R., CHERIN, E., GOERTZ, D. E. & FOSTER, F. S. 2010. Nonlinear emission from individual bound microbubbles at high frequencies. *Ultrasound in Medicine and Biology,* 36**,** 313-24.

TAKALKAR, A. M., KLIBANOV, A. L., RYCHAK, J. J., LINDNER, J. R. & LEY, K. 2004. Binding and detachment dynamics of microbubbles targeted to P-selectin under controlled shear flow. *Journal of Controlled Release,* 96**,** 473-482.

UNGER, E., MATSUNAGA, T. O., SCHUMANN, P. A. & ZUTSHI, R. 2003. Microbubbles in Molecular Imaging and Therapy. *Medica Mundi,* 47**,** 58.

VOS, H. J., DOLLET, B., BOSCH, J. G., VERSLUIS, M. & DE JONG, N. 2008. Nonspherical Vibrations of Microbubbles in Contact with a Wall--A Pilot Study at Low Mechanical Index. *Ultrasound in Medicine & Biology,* 34**,** 685-688.

YAMAKOSHI, Y. & MIWA, T. 2009. Microbubble Adhesion to Target Wall by Ultrasonic Wave Frequency Sweep Method. *Japanese Journal of Applied Physics,* 48.

ZHAO, S., BORDEN, M., BLOCH, S. H., KRUSE, D., FERRARA, K. W. & DAYTON, P. A. 2004a. Radiation-force assisted targeting facilitates ultrasonic molecular imaging. *Mol Imaging,* 3**,** 135-48.

ZHAO, S. K., BORDEN, M., BLOCH, S. H., KRUSE, D. E., FERRARA, K. W. & DAYTON, P. A. 2004b. Increasing binding efficiency of ultrasound targeted agents with radiation force. *2004 IEEE Ultrasonics Symposium, Vols 1-3***,** 1114-1117
2333.

ZHAO, S. K., KRUSE, D. E., FERRARA, K. W. & DAYTON, P. A. 2006. Acoustic response from adherent targeted contrast agents. *Journal of the Acoustical Society of America,* 120**,** El63-El69.